JOURNAL OF CHEMICAL & ENGINEERING DATA

ARTICLE

pubs.acs.org/jced

Experimental and Modeling Study of Methane Adsorption on Activated Carbon Derived from Anthracite

Jingjie Luo,[†] Yuefeng Liu,[†,‡] Chengfa Jiang,[*,†] Wei Chu,[*,†] Wen Jie,[†] and Heping Xie[§]

[†]Department of Chemical Engineering, Sichuan University, Chengdu 610065, China

[‡]Laboratoire des Matériaux, Surfaces et Procédés pour la Catalyse, UMR 7515 du CNRS, Université de Strasbourg, 67087 Strasbourg Cedex 08, France

[§]State Key Laboratory of Hydraulics and Mountain River Engineering, Sichuan University, Chengdu 610065, China

ABSTRACT: Low-cost anthracite was used as the raw material for preparing microporosity controlled activated carbons by KOH activation. The adsorption characteristics of methane onto activated carbon were measured at 298 K and pressures up to 3.5 MPa by a volumetric method. The experimental data were fitted to the Dubinin−Astakhov model, and relative deviations of better than 0.1 % were obtained. Three main factors were suggested, accounting for the higher methane uptake. It was revealed that better methane uptake is dependent on larger micropore volume and specific surface area. When the micropore volume and surface area of two samples are similar, the activated carbon possessing a narrower micropore size distribution performed higher methane uptake. The relationship between the surface coverage (C/C_0) and the isosteric heat of adsorption confirmed that the heterogeneities of the as-obtained samples was a main factor influencing the methane adsorption at a surface coverage lower than 0.7. The activated carbon possessing higher heterogeneity deserved better methane uptake. The kinetics of methane adsorption on five activated carbons obeyed the pseudosecond-order equation very well under current experimental conditions (298 K, 0.28 MPa). The activated carbon displayed a faster adsorption rate and possessed a better adsorption capacity of methane.

1. INTRODUCTION

As a main component of natural gas and coal bed gas, methane is viewed as a alternative fuel for petroleum products, a beneficial source for environmental and energy condensation from methane combustion, and an important dissolvent for organic matter.[1,2] In the past decade, there has been an enhancing interest in the development of transportable systems for methane storage. Among different approaches, adsorbed natural gas (ANG) is one of the prevalent method for the storage of methane. Compared with the high-pressure compressed natural gas (CNG) and the low-temperature liquid natural gas (LNG) approaches, the ANG process transforms the harsh operative conditions to (3 to 4) MPa and mild temperatures.[3,4] The adsorption of gas is a phenomenon generated from the interaction between adsorbent and adsorbate molecules.[5] Different adsorption processes call for different adsorption theory, which is essential for the improvement of the available application of methane resources. Understanding the adsorption processes in porous materials is a fundamental step in designing adsorption for gas storage. The Dubinin−Astakhov (DA) model and Toth model are two mature theories presently widely used for the gas adsorption onto microporous adsorbents, which are evidenced to be more accurate.[6−8]

Activated carbons possess large amounts of micropore volume, a highly heterogeneous surface, and easily tunable microporosity by chemical treatment and can be cheaply manufactured in large quantities.[9−11] They have become one of the most favorable adsorbents for the investigation of gas adsorption. Several investigations have been focused on how to enhance the methane uptake of adsorbents by chemical and physical pretreatment. On the other hand, plenty of investigations were committed into the aspect of the microstructure of activated carbon and their relationship with adsorption capacity of adsorbates.[12,13] It was reported that the general slit-like microporous structures of activated carbons were the principle sources of the structural irregularity and heterogeneity.[14] Zhou and co-workers[5,15] found a linear relationship between the micropore volume and the methane adsorption capacity. Machnikowski and co-workers[16] made some investigations on the activated carbons. They found out that the satisfactory performance was a result from the balance of the microporosity development and packing density. However, although the methane adsorption capacity has been widely put into investigations, the factors influencing the methane adsorption and how such procedures are implemented still call for further investigation.

In this paper, we prepare a series of activated carbons with controllable microporosity using chemical activation. The data of adsorption equilibrium will be measured via a volumetric method and fitted by using the DA model. The relationship between the microporosity and the methane adsorption capacity will be studied. The isosteric heat of adsorption will also be evaluated and discussed. To understand the kinetics of methane adsorption, the experimental data are modeled by the pseudofirst-order equation, pseudosecond-order equation, and the Elovich equation. Such a basic experimental investigation of methane adsorption onto activated carbons is useful for designing an efficient ANG storage system.

Special Issue: Kenneth N. Marsh Festschrift

Received: July 30, 2011
Accepted: October 31, 2011
Published: November 09, 2011

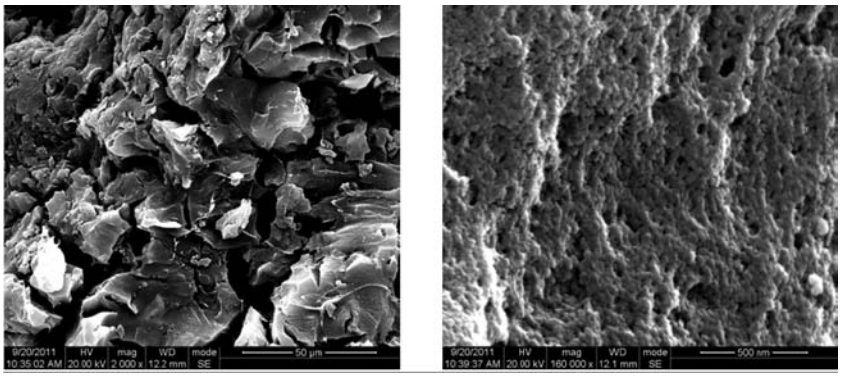

Figure 1. SEM profiles of the typical AC4 sample.

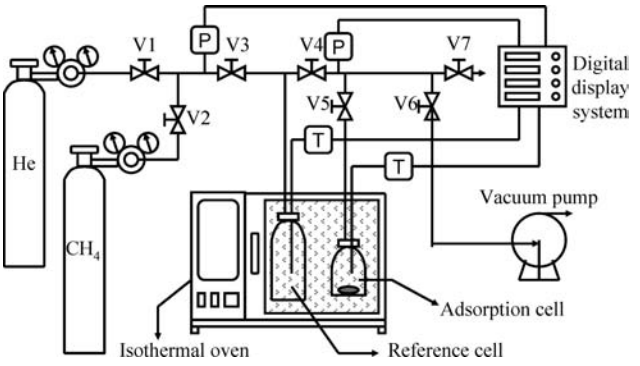

Figure 2. Schematic arrangement of the experimental setup. V, needle valve, P, pressure transducer; T, thermocouple.

2. EXPERIMENTAL SECTION

2.1. Materials. The activated carbons used were manufactured from fresh anthracite obtained (from the coal mine of Shanxi, China) by KOH activation. The anthracite was first crushed and sieved to particles of (20 to 40) mesh, washed by boiled water for 2 h, filtered with hot water, and dried in a furnace at 383 K overnight. After an aqueous solution of KOH was mixed with the anthracite powder, the mixture was immediately transferred into a ceramic boat and heated in a tubular furnace (model SK2-60-10HBP) under nitrogen flow. The temperature of the furnace was warmed up at a rate of 5 $K \cdot min^{-1}$ until 1023 K and maintained for 1 h. After cooled down to the room temperature, the powders were then washed by 5 $mol \cdot L^{-1}$ HCl aqueous solution and deionized water until the pH of the solution is about 7. After being filtered and dried in a furnace at 383 K overnight, the activated carbon was obtained. The as-prepared five activated carbons were denoted as AC1, AC2, AC3, AC4, and AC5 according to KOH/anthracite weight ratio (1:1, 2:1, 3:1, 4:1, and 5:1), respectively. The morphology and structure of the catalyst were studied using a scanning electron microscope (SEM, JEOL/EO, JSM-5900) as shown in Figure 1. The porous structures of these samples were determined using a NOVA1000e instrument of Quantachrome Company. The data of the related samples were obtained by N_2 adsorption at 77 K after degassed at 573 K for 180 min. The procedure is the same as in a previous paper.[17] The specific surface area was calculated from the Langmuir method;[18] the micropore volume was measured by the Dubinin−Radushkevich (DR) equation,[19] and the pore size distribution was calculated from the DA method.[20]

2.2. Experimental Apparatus and Methods. The methane isotherms were measured by a volumetric method by using a gas sorption apparatus (JWZZ-2F); the schematic arrangement is shown in Figure 2. The sample cell containing 1 g of powdered activated carbon was measured under pressures up to 3.5 MPa. Before the measurement, the sample was dried at 383 K in a vacuum furnace for at least 12 h. The tested sample was then immediately transferred into the adsorption cell and regenerated by degassing for about 3 h. The measurements were operated under 298 K.

Before the tested gas was entered into the adsorption apparatus, the needle valves V3 to V7 were kept closed. The reference cell and adsorption cell were kept at the required temperature using an isothermal furnace with error of ± 0.1 %. When the temperatures became stable, the pure gas was ventilated into the reference cell by opening V3 and V4. V3 was closed when the gas was enough for testing. After the initial pressure held steady and was recorded, the gas was entered into the adsorption cell via V5. The equilibrium was reached when the data from the pressure transducer remained the same for more than 10 min. After the cells reached the equilibrium, the final total pressure of the reference and adsorption cells was recorded. The V4 was closed, and the V7 was opened for the gas released from higher pressure. The vacuum pump was then used for half an hour to eliminate the gas adopted in the activated carbon. The amount of the gas occupied in the free space could then be calculated from the balance between the initial and the final pressures under the same temperature conditions. The same procedure was repeated to obtain various plots of gas amounts against the operating pressures. Each of the tests was operated twice to ensure the veracity of the experiment.

Helium Calibration and Methane Isotherm. The free space in the adsorption apparatus was corrected by the helium calibration. Since the helium is not adsorbed in the activated carbon (p < 10 MPa), it was usually used for the calibration of the free space in the apparatus. The purity of the helium is 99.999 %. The amounts of helium held in the free space of the apparatus as a function of pressure are listed in Figure 3. The measurement of methane isotherm was general, similar to that of the helium calibration. The helium was replaced by methane with a purity of 99.999 % before the operation.

Data Reduction. For the calculation of excess adsorption amount of methane (n_{exc}), the void volume of the adsorption apparatus is computed by the helium calibration data:

$$n_{void,\,He}(p,T) = (\rho_{ref}(p_{ref},T_{ref}) - \rho_{ads}(p_{ads},T_{ads}))V_{ref} \quad (1)$$

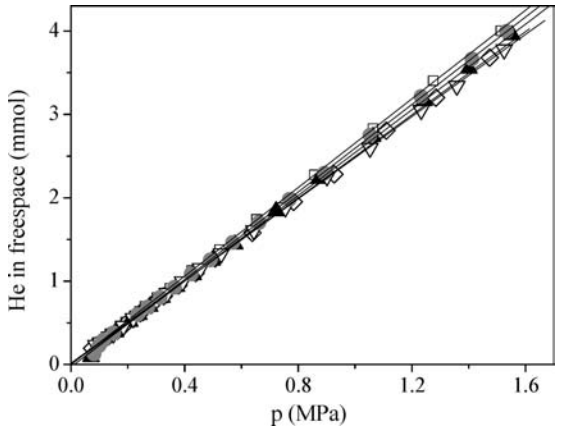

Figure 3. Helium calibration curves at 298 K of five activated carbons. □, AC1; ◇, AC2; ▲, AC3; ▽, AC4; and ●, AC5.

The $n_{void,He}$ (in moles) is the adsorption of void volume in the adsorption apparatus tested by the helium. The ρ_{ref}, p_{ref}, and T_{ref} are the density (in mol·m^{-3}) of helium in the reference cell condition, the pressure, and temperature of the reference cell. The ρ_{ads}, p_{ads}, and T_{ref} are the corresponding parameters in the adsorption cell.

According to the calcination methods by Wang et al.,[3] the void volume corresponding to the methane can be calculated from:

$$k = \frac{n_{void,CH_4}}{n_{void,He}} = \frac{\rho_{CH_4}}{\rho_{He}} \tag{2}$$

The n_{exc} in mol·kg^{-1} is obtained from:

$$n_{exc} = [(\rho'_{ref}(p_{ref}, T_{ref}) - \rho'_{ads}(p_{ads}, T_{ads}))V_{ref} - k \cdot n_{void,He}(p, T)]/m_{catal} \tag{3}$$

The parameters ρ' are densities of methane at the corresponding conditions. The m_{catal} is the mess of the catalyst, which is 1.0 g in this work.

The difference between the excess adsorption amount (n_{exc}) and the absolute adsorption amount (n_{abs}) is one of the factors impacting the accuracy of isotherm measurements. Under higher operative pressures, such a difference becomes apparent. As an indispensable factor, the n_{abs} is applied for evaluating the thermodynamic property of adsorbed phase. However, the n_{abs} revealing the true mass confined in the adsorbed phase cannot be directly measured. The so-called excess adsorption amount n_{exc} is approached from the experimental equilibrium data, which is used for the calculation of n_{abs} by the Gibbs equation for satisfying the theoretical analysis:

$$n_{exc} = n_{abs} - v_a\rho_g \tag{4}$$

$$n_{exc} = n_{abs} - v_a\rho_g = v_a\rho_a - v_a\rho_g = n_{abs}(1 - \rho_g/\rho_a) \tag{5}$$

$$n_{abs} = \frac{n_{exc}}{(1 - \rho_g/\rho_a)} \tag{6}$$

in which the v_a is the volume of adsorbed phase, m^3·kg^{-1}, and the ρ_g and ρ_a are the density of the free gas phase and the gas in the adsorbed state, mol·m^{-3}. The calculation of n_{abs} in mol·kg^{-1} from the n_{exc} and ρ_a usually causes the initial uncertainty of the data from the different approaches. Here the equations suggested by Ozawa and Dubinin[21,22] are applied for calculating the ρ_a and quasi-saturated vapor pressure (p_s) which were proved to be more accurate.[23]

Ozawa and co-workers:

$$\rho_a = \rho_b \exp[-0.0025(T - T_b)] \tag{7}$$

Dubinin and co-workers:

$$p_s = p_c(T/T_c)^2 \tag{8}$$

In the above equations, subscript b refers to the normal boiling point of methane. p_c and T_c are the critical properties of methane. For the sake of model application, the kg·kg^{-1} is used for the amount adsorbed in measurements instead of mol/kg as mentioned in the following part.

The density of the methane in free gas phase (ρ_g) was calculated by the Peng−Robinson (PR) equation:

$$p = \frac{RT}{V_m - b} - \frac{a\alpha}{V_m^2 + 2bV_m - b^2} \tag{9}$$

The A and B parameters are defined as:

$$A = \frac{a\alpha p}{R^2T^2} \quad \text{and} \quad B = \frac{bp}{RT} \tag{10}$$

$$\text{where } a = \frac{0.457235R^2T_c^2}{p_c} \quad \text{and} \quad b = \frac{0.077796RT_c}{p_c} \tag{11}$$

$$\alpha = (1 + m(1 - T_r^{0.5}))^2 \tag{12}$$

$$m = 0.37464 + 1.54226\omega - 0.26992\omega^2 \tag{13}$$

$$T_r = T/T_c \tag{14}$$

The density of the free gas can be expressed as:

$$\rho = \frac{P}{ZRT}(\text{mol}\cdot\text{m}^{-3}) \tag{15}$$

in which Z is the compressibility factor and P and T are the pressure (kPa) and the temperature (K).

Z is obtained by solving the following equation using the iteration method:

$$Z^3 - (1 - B)Z^2 + (A - 2B - 3B^2)Z - (AB - B^2 - B^3) = 0 \tag{16}$$

In this case, the density of the free gas phase can be then obtained.

The experimental isotherms are correlated with the DA model, which has been widely used for IUPAC Type I isotherms and is typical physisorption of several gases on activated carbons.[4,7,8]

The DA equation has the following form:

$$W = W_0 \exp\left(-\left[\frac{RT}{E}\ln\left(\frac{p_s}{p}\right)\right]^t\right) \tag{17}$$

$$W = Cv_a \tag{18}$$

where W is the volume uptake of methane in cm^3·g^{-1}, W_0 is the saturated volume uptake of methane in the adsorption space in cm^3·g^{-1}, E is the characteristic energy of the adsorption

system, t refers to the structural heterogeneity factor, and C is the methane adsorption amount in $kg \cdot kg^{-1}$. The v_a is the adsorbed phase specific volume which can be estimated as below:

$$v_a = v_b \exp[\alpha(T - T_b)] \quad (19)$$

where the subscript b refers to the normal boiling point of methane, and α can be calculated by $1/T$.[24]

The prediction uncertainty is determined by the mean relative deviation δ:

$$\delta = \sqrt{\frac{1}{N}\sum_{i=1}^{N}\left(\frac{n_{abs,i} - n_{cal,i}}{n_{abs,i}}\right)^2} \quad (T = 298\ K) \quad (20)$$

where N is the number of data points.

2.3. Kinetic Modeling. *Pseudofirst-Order Model.* The pseudo-first-order rate equation is expressed as:

$$\frac{dq_t}{dt} = k_1(q_{e,1} - q_t) \quad (21)$$

where $q_{e,1}$ ($kg \cdot kg^{-1}$) is applied for the amount of methane adsorbed onto the activated carbon at equilibrium according to the pseudofirst-order model, q_t is the methane uptake at corresponding time t (s), and k_1 is the rate constant (1/s) of the pseudofirst-order model adsorption.[25] After integration by applying the initial conditions $q_t = 0$ at $t = 0$ and $q_t = q_t$ at $t = t$, it turns out to be:

$$\log(q_{e,1} - q_t) = \log q_{e,1} - \left(\frac{k_1}{2.303}\right)t \quad (22)$$

If the methane adsorption obeys the pseudofirst-order model, the plots of $\log(q_{e,1} - q_t)$ versus t should be linear.

Pseudosecond-Order Model. The pseudosecond-order rate equation is shown as below:

$$\frac{dq_t}{dt} = k_2(q_{e,2} - q_t)^2 \quad (23)$$

Applying the above-mentioned initial conditions, the integration equation can be described as:

$$\frac{t}{q_t} = \frac{1}{k_2 q_{e,2}^2} + \left(\frac{1}{q_e}\right)t \quad (24)$$

In this model, the $q_{e,2}$ in $kg \cdot kg^{-1}$ and k_2 in $kg \cdot kg^{-1} \cdot s^{-1}$ are the amount of methane adsorbed at equilibrium and rate constant according to the pseudosecond-order model adsorption, respectively.[26]

Elovich Model. The experimental data are also analyzed by the Elovich model,[27] which has the following linear form:

$$q_t = (1/\beta)\ln(\alpha\beta) + (1/\beta)\ln t \quad (25)$$

where the parameter α is the initial rate constant, and β reveals the extent of C/C_0 and activation energy.

3. RESULTS AND DISCUSSION

3.1. Porous Structure of the Anthracite-Based Activated Carbon. The N_2 adsorption isotherms of the five activated carbons are presented in Figure 4. All of the five samples possess a Type I adsorption isotherm according to the IUPAC classification, a characteristic curve of material with micropores.[28] It is obvious that the N_2 uptakes of samples urgently increase with the pressures in lower relative pressure range ($P/P_0 < 0.2$), which is attributed to the volume filling and monolayer distribution processes of micropores. After the knee of the adsorption isotherm, a general flat stage with minimal slope then appears, providing a profile of the sample structures with mainly micropores. Among the five activated carbons, the AC1 activated carbon displays much lower N_2 uptake, indicating that the lower alkali/anthracite weight ratio causes incomplete development of microporosity in the AC1 activated carbon. The nitrogen adsorption amount evidently rises along with the alkali/anthracite weight ratio until it reaches 5:1. The sharp drop of the nitrogen uptake over the AC5 sample maybe resulted from the superfluous alkali poisoning. The AC4 sample displays a higher N_2 uptake compared with the other samples. The correlated average pore diameter of all of the five samples fall in the range of micropores (< 2 nm).

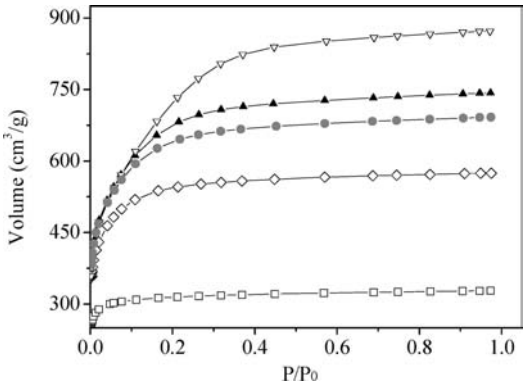

Figure 4. N_2 adsorption isotherms (77 K) corresponding to the five activated carbons. □, AC1; ◇, AC2; ▲, AC3; ▽, AC4; and ●, AC5.

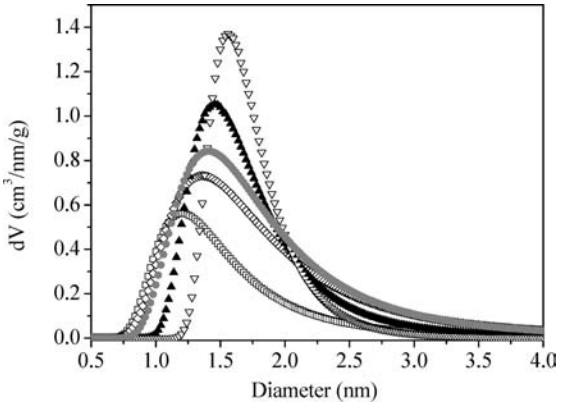

Figure 5. Pore size distribution obtained applying the DA equation to the N_2 adsorption data. □, AC1; ◇, AC2; ▲, AC3; ▽, AC4; and ●, AC5.

The pore size distribution obtained by applying the DA equation to the N_2 adsorption data is shown in Figure 5. The corresponding texture parameters are listed in Table 1. The pores in the samples generally lie in the microporous range (<2 nm). It can be seen that the higher the alkali amount is, the narrower the pore size distribution develops, except for the AC5 activated carbon. The AC4 sample displays a narrow and sharp increase of micropore volume. However, the average pore diameter also increases along with the alkali/anthracite weight ratio. It is noteworthy that, after the alkali/anthracite weight ratio reaches 3:1, the specific surface area and the micropore volume differ not

Table 1. Porous Properties of the Five Activated Carbons

	S_{BET}	V_{micro}	average pore diameter
sample	$m^2 \cdot g^{-1}$	$cm^3 \cdot g^{-1}$	nm
AC1	1265	0.483	1.18
AC2	1894	0.756	1.36
AC3	2082	0.841	1.40
AC4	2071	0.833	1.40
AC5	2075	0.851	1.48

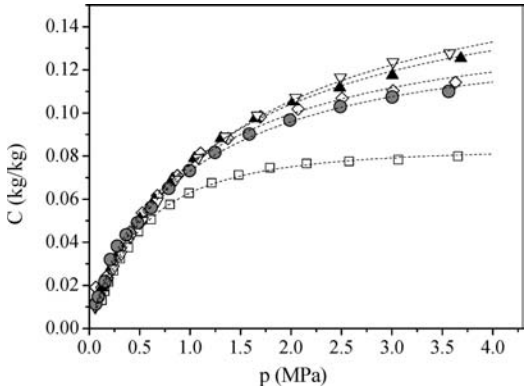

Figure 6. Equilibrium isotherms of methane adsorption on five activated carbons at 298 K. □, AC1; ◇, AC2; ▲, AC3; ▽, AC4; and ●, AC5; and dotted line, DA model.

obviously along with the alkali/anthracite weight ratio. Comparing with the AC3 and AC4 activated carbons, the pore size distribution of AC5 sample becomes wider and the tail largely dragged into the range of mesopore.

3.2. Adsorption of Methane on Five Activated Carbons. The equilibrium data of methane adsorption at 298 K and pressures up to 3.5 MPa are collected by the volumetric method as shown in Figure 6. The experimental uptake of methane profile characteristic of type I adsorption isotherm according to the IUPAC classification is observed. At lower relative pressures, the amounts of the methane uptake drastically increase but then slowly increase with the further rise of pressure, as reported previously.[10,29] The methane adsorptions on the activated carbons do not complete in the operative condition except for the AC1 activated carbon. The methane adsorption measurements show that the AC1 and AC4 activated carbons perform the least and most methane uptakes among the five samples, respectively. By the way, although the specific surface area and the micropore volume of the AC3, AC4, and AC5 samples are similar, the methane storage capacity differs from each other, especially for the AC5 sample. Combined with the N_2 adsorption tests, the AC4 sample with a narrower pore size distribution displays better methane adsorption ability. The pore size distributions of the AC3 and AC5 samples are broader and dispersed. For the AC5 sample, the aggressive activation even causes the transition from micropore to mesopore as mentioned above. It was previously considered that the favorable pore size for methane adsorption is about 0.8 nm,[13] and a suited average pore diameter was more available for the delivery and adsorption of methane. The much larger diameter of the activated carbon micropores can easily induce the desorption of the methane. From the methane adsorption measurements, it is concluded that the methane

Table 2. Adsorption Parameters of the DA Model of Methane Adsorption Equilibrium over Five Activated Carbons at 298 K

DA model	AC1	AC2	AC3	AC4	AC5
W_0 ($m^3 \cdot kg^{-1}$)	0.22	0.35	0.39	0.41	0.33
E ($kJ \cdot mol^{-1}$)	9.14	8.10	7.5	7.2	8.1
t	3.10	1.99	1.87	1.89	2.07
mean relative deviation δ (%)	$1.4 \cdot 10^{-4}$	$8.0 \cdot 10^{-4}$	$1.3 \cdot 10^{-4}$	$8.9 \cdot 10^{-4}$	$4.5 \cdot 10^{-4}$

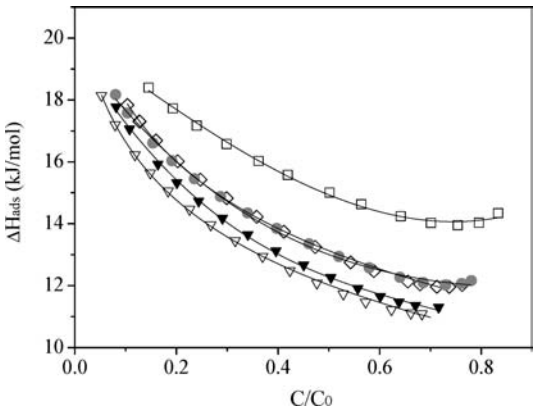

Figure 7. Uptake dependence of isosteric heat of adsorption derived from the DA model. □, AC1; ◇, AC2; ▲, AC3; ▽, AC4; and ●, AC5.

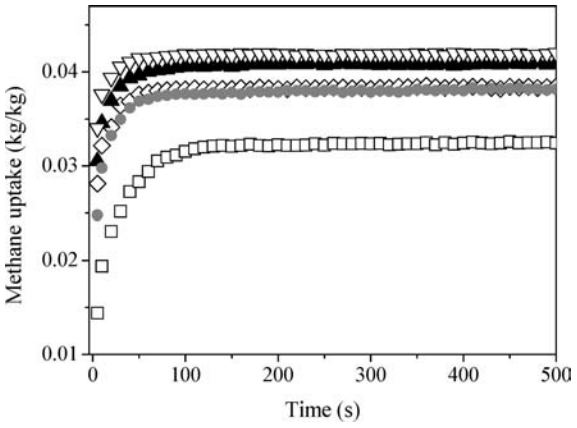

Figure 8. Adsorption kinetics plots of methane on five activated carbons. Initial pressure: 0.28 MPa. Temperature: 298 K; □, AC1; ◇, AC2; ▲, AC3; ▽, AC4; and ●, AC5.

adsorption on the five activated carbons increases along with the micropore volume and the surface area. When the micropore volume and surface area of the materials are considerable, the width of the pore size distribution is a more sensitive factor. The narrower the pore size distribution, the better the methane adsorption capacity.

The experimental data are fitted by the DA model (dotted lines). It can be seen that the DA plots fit the data well. The parameters and mean relative deviation obtained from the DA model are listed in Table 2. The calculated relative deviations δ of all of the activated carbons are lower than 0.1 %. The interesting part is that the obtained t value from the DA model regularly decreases along with the increase of the calculated W_0. It was

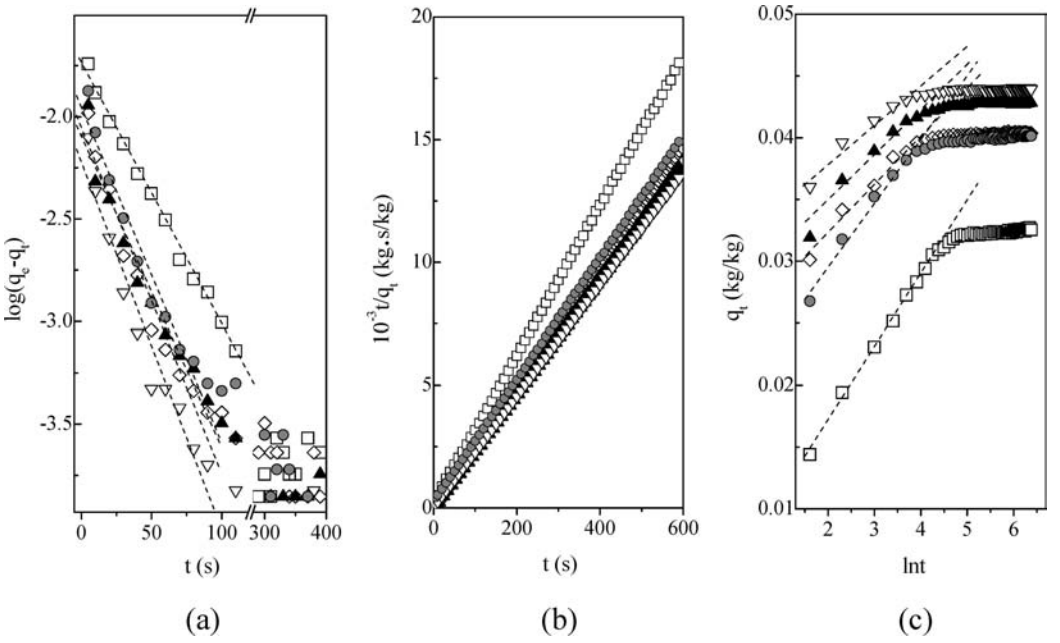

Figure 9. Methane adsorption kinetic plots over five activated carbons according to the pseudofirst-order kinetics (a); the pseudosecond-order kinetics (b); and the Elovich equation (c). □, AC1; ◇, AC2; ▲, AC3; ▽, AC4; and ●, AC5.

reported that the t values from the DA model are inversely proportional to the magnitude of the fractal dimensions that determine the surface irregularity.[30] In this way, the AC3 and AC4 activated carbons with a lower t value possess the most heterogeneous microstructures.

For ideal adsorption process, the isosteric heat of adsorption (ΔH_{ads}) is constant with the variation of C/C_0. However, for some adsorbent materials such as anthracite and activated carbon that possess a heterogeneous surface, the ΔH_{ads} are essential for the adsorption of methane and other gases. For the nonideality of the gas phase, the isosteric heat of adsorption changes greatly with C/C_0.[4,31] Therefore in this work, ΔH_{ads} is extracted by Clausius−Clapeyron equation from the experimental data:

$$\Delta H_{ads} = -R\frac{\partial \ln p}{\partial(1/T)}\bigg|_n \tag{26}$$

according to the expression of the DA equation, ΔH_{ads} can be extracted from below:

$$\Delta H_{ads} = 2RT + E\left[\left(\ln\left(\frac{W_0}{Cv_a}\right)\right)^{1/t} + \frac{\alpha T_b}{t}\ln\left(\frac{W_0}{Cv_a}\right)^{1-t/t}\right] \tag{27}$$

Figure 7 shows the uptake dependence of ΔH_{ads} on activated carbon. As it is shown in Figure 7, ΔH_{ads} varies largely with C/C_0. Before the C/C_0 reaches about 0.7, the value of the ΔH_{ads} over the five activated carbons all decrease with the increase of the C/C_0. However, the plots of the AC1, AC2, and AC5 activated carbons then tend to boost a little with the further increase of the C/C_0 ($C/C_0 > 0.7$). It was reported that the variation of the ΔH_{ads} versus the C/C_0 reflected the interaction relationship between the adsorbent and adsorbate molecules. During the initial stage of methane adsorption, the apparent decrease of the ΔH_{ads} with C/C_0 suggests that the energetic heterogeneity is the initial dynamic for the methane adsorption under current experimental conditions,[8] and the interaction between adsorbent and adsorbate is stronger.[32] Such analysis is in consistence with the result from Figure 6 that the most heterogeneous AC3 and AC4 activated carbons perform better adsorption capacity of methane than the others. The boosting of the plots at higher surface coverage (>0.7) illustrates that the interaction between adsorbent and adsorbate is weaker. The main factor near equilibrium influencing the methane adsorption transfers into the adsorbate interaction.

3.3. Adsorption Kinetics. The adsorption kinetic plots of methane on five anthracite-based activated carbons under 0.28 MPa are shown in Figure 8. It can be seen that the AC1 sample possesses the lowest methane uptake among the five samples under the same operation conditions. The saturated amounts of methane adsorption on the activated carbons rise along with increase of the alkali/anthracite weight ratio. Comparing with the AC4 sample, the AC5 sample displays a drop of the adsorption capacity. Besides, each of the samples rapidly reaches their equilibrium after the adsorption begins except the AC1 sample, which reaches the equilibrium with tardiness at more than 100 s.

To understand the controlling mechanism of sorption process such as mass transfer and chemical reaction, the different kinetic models are applied in this study. Recently, the pseudofirst-order equation and pseudosecond-order equation have been widely used for the investigations of the adsorption between gases and solids.[25,26,33,34] An earlier investigation of our group has also evidenced the applicability of pseudosecond-order kinetics over gas adsorbed onto activated carbon.[9] In addition, the Elovich equation is one of the equations successfully expressing the activated chemisorptions.[35,36]

The methane adsorption kinetic plots over five activated carbons according to the above-mentioned three models are shown in Figure 9a−c. The corresponding parameters can be obtained from the linear relationship between the x and y coordinate axes as listed in Table 3. It can be seen from Figure 9a that

Table 3. Kinetic Parameters for the Methane Adsorption on Five Activated Carbons under 0.28 MPa

		pseudofirst-order kinetic model			pseudosecond-order kinetic equation			Elovich equation		
	$q_{e,exp}$	$q_{e,1}$	k_1		$q_{e,2}$	k_2				
	kg·kg^{-1}	kg·kg^{-1}	s^{-1}	R_1^2	kg·kg^{-1}	kg·g^{-1}·s^{-1}	R_2^2	α	β	R_E^2
AC1	0.0325	0.01840	0.0301	0.996	0.0329	5.60	0.999	0.015	169.49	0.999
AC2	0.0405	0.00888	0.0389	0.981	0.0405	21.44	0.999	2.207	264.55	0.988
AC3	0.0429	0.00806	0.0350	0.976	0.0429	22.12	0.999	5.283	265.96	0.986
AC4	0.0439	0.00600	0.0413	0.974	0.0440	37.68	0.999	74.660	318.47	0.982
AC5	0.0401	0.0111	0.0377	0.981	0.0403	9.22	0.999	0.206	192.31	0.992

the kinetic plots present a general linear relationship with time before the methane adsorption reaches the equilibrium. From the calculated results, although a linear relationship exists, the calculated saturated methane adsorption amounts differ much from those experimental data, and the variation trend of the calculated value changes differently from the experimental results. Hence, the pseudofirst-order equation is not appropriate for the application of the methane adsorption on the five activated carbons. The pseudosecond-order equation fits the experimental data very well as illustrated in Figure 9b, and the R^2 for all the samples are about 0.999. The kinetic plots of q_t versus ln t according to the Elovich equation are linear from the beginning of adsorption until adsorbent loadings up to 80 % of the equilibrium value.[37] The fitting results suggest that the pseudosecond-order adsorption mechanism is predominant. The kinetics of adsorption complies with a second-order rate law with respect to the availability of adsorption sites on the adsorbent surface rather than adsorbate concentration.[38]

From the results of Figure 9b and Table 3, good consistency exists between the saturated methane adsorption amounts of experimental and calculated values from the pseudosecond-order equation. The slope of the kinetic plots of the AC4 sample is obvious larger than the other samples. The AC1 sample displays the lowest adsorption rate constant. With the rising of the alkali concentration, the calculated saturated adsorption amount coherently increases as the same trend of the experimental data. The rate constant of the methane adsorption on the AC4 activated carbon even increases to 37.68 kg·g^{-1}·s^{-1}. The adsorption rates of activated carbons are thus apparently enhanced. This phenomenon may be attributed to the favorable micropore volume and diameter generated from the feasible activation process, which facilitate the delivery and adsorption of methane in the pores of activated carbon. From Table 3, it can be seen that, although the saturated adsorption amount of the AC2 and AC5 samples are similar, the rate constant greatly changes. This can be ascribed from the generation of more mesopores during the aggressive activation. The methane molecular adsorbed on the mesopores can be easily desorbed due to the wider pore diameter in the AC5 sample, causing the sluggish of the adsorption rate.

It is noticeable that, according to the previous report by He and co-workers,[39] the initial pressure should be taken into consideration when calculating the adsorption kinetics. The above investigation of methane adsorption kinetics is under the current experimental condition (298 K, 0.28 MPa). The investigation of how the factors including initial pressure influencing the adsorption kinetics of methane is the further work we are taking part in.

4. CONCLUSION

In this work, five activated carbons were derived from very low cost anthracite and activated by KOH activation. The N_2 adsorption isotherms informed the controllable micropore structures of the as-prepared activated carbons. The methane adsorption capacities of the activated carbons were tested by a volumetric method and fitted by the DA model. It was suggested that the investigation drawn forth several reasons for a better adsorption capacity of methane as listed below: (i) The better methane adsorption capacity was relative to the larger micropore volume and specific surface area. When the above microporosity parameters of two samples were similar, the methane adsorption capacity depended on the micropore size distribution. The narrower micropore size distribution facilitated the methane adsorption. (ii) The calculated parameter of DA model suggested that the AC4 activated carbon possesses a most heterogeneous structure, which was confirmed to be one of the reasons accounting for better methane adsorption capacity. (iii) The kinetics of methane adsorption revealed that such process obeyed the pseudosecond-order model very well under current experimental condition (298 K, 0.28 MPa). The AC4 activated carbon with a better methane adsorption capacity performed at a faster adsorption rate.

AUTHOR INFORMATION

Corresponding Author

*Tel.: +86-28-85403836. Fax: +86-28-85461108. E-mail: jiangcf1@yahoo.com (C.F.J.); chuwei65@yahoo.com.cn (W.C.).

Funding Sources

This work was financed under National Basic Research Program of China (973 Program) (2011CB201202).

ACKNOWLEDGMENT

The authors also thank Wenjing Sun and Ning Wang for their helpful discussions.

REFERENCES

(1) Alcañiz-Monge, J.; De La Casa-Lillo, M. A.; Cazorla-Amorós, D.; Linares-Solano, A. Methane Storage in Activated Carbon Fibres. *Carbon* **1997**, *35* (2), 291–297.

(2) Shi, L. M.; Chu, W.; Qu, F. F.; Luo, S. Z. Low-temperature Catalytic Combustion of Methane over MnO_x-CeO_2 Mixed Oxide Catalysts: Effect of Preparation Method. *Catal. Lett.* **2007**, *113* (1), 59–64.

(3) Wang, X. L.; French, J.; Kandadai, S.; Chua, H. T. Adsorption Measurements of Methane on Activated Carbon in the Temperature

Range (281 to 343) K and Pressures to 1.2 MPa. *J. Chem. Eng. Data* **2010**, *55* (8), 2700–2706.

(4) Rahman, K. A.; Loh, W. S.; Yanagi, H.; Chakraborty, A.; Saha, B. B.; Chun, W. G.; Ng, K. C. Experimental Adsorption Isotherm of Methane onto Activated Carbon at Sub- and Supercritical Temperatures. *J. Chem. Eng. Data* **2010**, *55* (11), 4961–4967.

(5) Zhou, Y. P.; Zhou, L. Fundamentals of High Pressure Adsorption. *Langmuir* **2009**, *25* (23), 13461–13466.

(6) Schindler, B. J.; Buettner, L. C.; Douglas LeVan, M. Transition to Henry's Law in Ultra-Low Concentration Adsorption Equilibrium for *n*-Pentane on BPL Activated Carbon. *Carbon* **2008**, *46* (10), 1285–1293.

(7) Siemons, N.; Busch, A. Measurement and Interpretation of Supercritical CO_2 Sorption on Various Coals. *Int. J. Coal Geol.* **2007**, *69* (4), 229–242.

(8) Himeno, S.; Komatsu, T.; Fujita, S. High-pressure Adsorption Equilibria of Methane and Carbon Dioxide on Several Activated Carbons. *J. Chem. Eng. Data* **2005**, *50* (2), 369–376.

(9) Wen, J.; Han, X.; Lin, H. G.; Zheng, Y.; Chu, W. A Critical Study on the Adsorption of Heterocyclic Sulfur and Nitrogen Compounds by Activated Carbon: Equilibrium, Kinetics and Thermodynamics. *Chem. Eng. J.* **2010**, *164* (1), 29–36.

(10) He, Y.; Seaton, N. A. Monte Carlo Simulation and Pore-Size Distribution Analysis of the Isosteric Heat of Adsorption of Methane in Activated Carbon. *Langmuir* **2005**, *21* (18), 8297–8301.

(11) Lee, Y. W.; Park, J. W.; Choung, J. H.; Choi, D. K. Adsorption Characteristics of SO_2 on Activated Carbon Prepared from Coconut Shell with Potassium Hydroxide Activation. *Environ. Sci. Technol.* **2002**, *36* (5), 1086–1092.

(12) Prinz, D.; Littke, R. Development of the Micro- and Ultramicroporous Structure of Coals with Rank as Deduced from the Accessibility to Water. *Fuel* **2005**, *84* (12−13), 1645–1652.

(13) Lozano-Castelló, D.; Cazorla-Amorós, D.; Linares-Solano, A.; Quinn, D. F. Influence of Pore Size Distribution on Methane Storage at Relatively low Pressure: Preparation of Activated Carbon with Optimum Pore Size. *Carbon* **2002**, *40* (7), 989–1002.

(14) Jaroniec, M. Physical Adsorption on Heterogeneous Solids--Present and Future. *Thin Solid Films* **1983**, *100* (4), 325–328.

(15) Sun, Y.; Liu, C. M.; Su, W.; Zhou, Y. P.; Zhou, L. Principles of Methane Adsorption and Natural Gas Storage. *Adsorption* **2009**, *15* (2), 133–137.

(16) Machnikowski, J.; Kierzek, K.; Lis, K.; Machnikowska, H.; Czepirski, L. Tailoring Porosity Development in Monolithic Adsorbents Made of KOH-Activated Pitch Coke and Furfuryl Alcohol Binder for Methane Storage. *Energy Fuels* **2010**, *24* (6), 3410–3414.

(17) Xu, J. Q.; Chu, W.; Luo, S. Z. Synthesis and Characterization of Mesoporous V-MCM-41 Molecular Sieves with Good Hydrothermal and Thermal Stability. *J. Mol. Catal. A* **2006**, *256* (1−2), 48–56.

(18) Gómez-Serrano, V.; González-García, C. M.; González-Martín, M. L. Nitrogen adsorption isotherms on carbonaceous materials. Comparison of BET and Langmuir surface areas. *Powder Technol.* **2001**, *116* (1), 103–108.

(19) Arami-Niya, A.; Daud, W. M. A. W.; Mjalli, F. S. Using Granular Activated Carbon Prepared from Oil Palm Shell by $ZnCl_2$ and Physical Activation for Methane Adsorption. *J. Anal. Appl. Pyrol.* **2010**, *89* (2), 197–203.

(20) Gil, A.; Korili, S. A.; Cherkashinin, G. Y. Extension of the Dubinin−Astakhov equation for evaluating the micropore size distribution of a modified carbon molecular sieve. *J. Colloid Interface Sci.* **2003**, *262* (2), 603–607.

(21) Ozawa, S.; Kusumi, S.; Ogino, Y. Physical Adsorption of Gases at High Pressure. IV. An Improvement of the Dubinin--Astakhov Adsorption Equation. *J. Colloid Interface Sci.* **1976**, *56* (1), 83–91.

(22) Dubinin, M. M. The Potential Theory of Adsorption of Gases and Vapors for Adsorbents with Energetically Nonuniform Surfaces. *Chem. Rev.* **1960**, *60* (2), 235–241.

(23) Li, M.; Gu, A. Z.; Lu, X. S.; Wang, R. S. Supercritical Methane Adsorption Equilibrium Data on Activated Carbon with Prediction by the Adsorption Potential Theory. *J. Chem. Eng. Data* **2004**, *49* (1), 73–76.

(24) Saha, B. B.; Koyama, S.; El-Sharkawy, I. I.; Habib, K.; Srinivasan, K.; Dutta, P. Evaluation of Adsorption Parameters and Heats of Adsorption through Desorption Measurements. *J. Chem. Eng. Data* **2007**, *52* (6), 2419–2424.

(25) Chauhan, K.; Chauhan, G. S.; Ahn, J. H. Novel Polycarboxylated Starch-Based Sorbents for Cu^{2+} Ions. *Ind. Eng. Chem. Res.* **2010**, *49* (6), 2548–2556.

(26) Nieszporek, K.; Banach, T. Influence of Energetic Heterogeneity and Lateral Interactions between Adsorbed Molecules on the Kinetics of Gas Adsorption. *Ind. Eng. Chem. Res.* **2011**, *50* (6), 3078–3088.

(27) Wu, F. C.; Tseng, R. L. High Adsorption Capacity NaOH-Activated Carbon for Dye Removal from Aqueous Solution. *J. Hazard. Mater.* **2008**, *152* (3), 1256–1267.

(28) Sonwane, C. G.; Bhatia, S. K. Characterization of Pore Size Distributions of Mesoporous Materials from Adsorption Isotherms. *J. Phys. Chem. B* **2000**, *104* (39), 9099–9110.

(29) Morales-Cas, A. M.; Moya, C.; Coto, B.; Vega, L. F.; Calleja, G. Adsorption of Hydrogen and Methane Mixtures on Carbon Cylindrical Cavities. *J. Phys. Chem. C* **2007**, *111* (17), 6473–6480.

(30) Erdem-Senatalar, A.; Tatller, M.; Sirkecioglu, A. The Relationship of the Geometric Factor in the Dubinin-Astakhov Isotherm Equation with the Fractal Dimension. *Colloids Surf., A* **2000**, *173* (1−3), 51–59.

(31) Loh, W. S.; Rahman, K. A.; Chakraborty, A.; Saha, B. B.; Choo, Y. S.; Khoo, B. C.; Ng, K. C. Improved Isotherm Data for Adsorption of Methane on Activated Carbons. *J. Chem. Eng. Data* **2010**, *55* (8), 2840–2847.

(32) Martin, A.; Loh, W. S.; Rahman, K. A.; Thu, K.; Surayawan, B.; Alhamid, M. I.; Nasruddin; Ng, K. C. Adsorption Isotherms of CH_4 on Activated Carbon from Indonesian Low Grade Coal. *J. Chem. Eng. Data* **2011**, *56* (3), 361–367.

(33) Özacar, M.; Sengil, I. A. A Kinetic Study of Metal Complex Dye Sorption onto Pine Sawdust. *Process Biochem.* **2005**, *40* (2), 565–572.

(34) Duran, C.; Ozdes, D.; Gundogdu, A.; Senturk, H. B. Kinetics and Isotherm Analysis of Basic Dyes Adsorption onto Almond Shell (Prunus dulcis) as a Low Cost Adsorbent. *J. Chem. Eng. Data* **2011**, *56* (5), 2136–2147.

(35) Wu, F. C.; Tseng, R. L.; Hu, C. C. Comparisons of Pore Properties and Adsorption Performance of KOH-Activated and Steam-Activated Carbons. *Microporous Mesoporous Mater.* **2005**, *80* (1−3), 95–106.

(36) Fernández-Bayo, J. D.; Nogales, R.; Romero, E. Evaluation of the Sorption Process for Imidacloprid and Diuron in Eight Agricultural Soils from Southern Europe Using Various Kinetic Models. *J. Agric. Food Chem.* **2008**, *56* (13), 5266–5272.

(37) Petrolekas, P. D.; Maggenakis, G. Kinetic Studies of the Liquid-Phase Adsorption of a Reactive Dye onto Activated Lignite. *Ind. Eng. Chem. Res.* **2007**, *46* (4), 1326–1332.

(38) Liu, Y. New Insights into Pseudo-Second-Order Kinetic Equation for Adsorption. *Colloids Surf., A* **2008**, *320* (1−3), 275–278.

(39) Ng, K. C.; He, J. M.; Yap, C.; Saha, B. B. Effect of Pressure on the Adsorption Rate for Gasoline Vapor on Pitch-Based Activated Carbon. *J. Chem. Eng. Data* **2009**, *54* (5), 1504–1509.